Proceedings of the ASME 2020 International Design Engineering Technical Conferences and Computers and Information in Engineering Conference IDETC/CIE2020 August 16-19, 2020, St. Louis, MO, USA

IDETC-19423

TIME-DEPENDENT SYSTEM RELIABILITY ANALYSIS WITH SECOND ORDER RELIABILITY METHOD

Hao Wu

Department of Mechanical and Energy Engineering Indiana University - Purdue University Indianapolis Indianapolis, IN

Xiaoping Du¹

Department of Mechanical and Energy Engineering Indiana University - Purdue University Indianapolis Indianapolis, IN

ABSTRACT

System reliability is quantified by the probability that a system performs its intended function in a period of time without failure. System reliability can be predicted if all the limit-state functions of the components of the system are available, and such a prediction is usually time consuming. This work develops a time-dependent system reliability method that is extended from the component time-dependent reliability method that uses the envelop method and second order reliability method. The proposed method is efficient and is intended for series systems with limit-state functions whose input variables include random variables and time. The component reliability is estimated by the existing second order component reliability method, which produces component reliability indexes. The covariance between components responses are estimated with the first order approximations, which are available from the second order approximations of the component reliability analysis. Then the joint probability of all the component responses is approximated by a multivariate normal distribution with its mean vector being component reliability indexes and covariance being those between component responses. The proposed method is demonstrated and evaluated by three examples.

Keywords: System reliability, Second order approximation, Envelope method, Numerical method

1. INTRODUCTION

System reliability is measured by the probability that the system performs its intended function in routine circumstances during a specified period of time [1]. It is necessary to predict system reliability accurately and efficiently in the early design stage since it can be used to estimate the lifecycle cost, determine maintenance policies, and optimize the system performance [2-4]. A mechanical system consists of multiple components, and each component may also have multiple failure modes. In this work, we consider a failure mode as a component. If the limitstate function of a failure mode is invariant over time, its reliability and probability of failure are constant. However, the limit-state function varies over time in many engineering problems, such as function generator mechanisms [5] and bridges under stochastic loading [6]. Then a time-dependent reliability method is required.

Suppose the limit-state function of the *i*-th failure mode is given by

$$Y_i = q_i(\mathbf{X}, t) \tag{1}$$

 $Y_i = g_i(\mathbf{X}, t) \tag{1}$ where Y_i is a component response and it varies with time t; and $\mathbf{X} = (X_1, ..., X_n)^{\mathrm{T}}$ is the vector of independent random variables. Then the time-dependent component reliability over a time interval $[t_0, t_s]$ is defined by

$$R(t_0, t_s) = \Pr(g(\mathbf{X}, t) \ge 0, \forall t \in [t_0, t_s])$$
 (2)

and the corresponding probability of failure is defined by

$$p_f(t_0, t_s) = \Pr(g(\mathbf{X}, t) < 0, \exists t \in [t_0, t_s])$$
 (3)

Eq. (3) indicates that if $g(\cdot) < 0$ occurs at any instant of time on $[t_0, t_s]$, the component fails.

In this study, we focus on series system. If one failure mode occurs, the entire system fails. For a time-dependent series system, if any failure mode occurs at any instant of time, the system fails. The system reliability $R_s(t_0, t_s)$ and probability of failure $p_{fs}(t_0, t_s)$ are given by

$$R_s(t_0, t_s) = \Pr\left(\bigcap_{i=1}^m g_i(\mathbf{X}, t_i) \ge 0, \forall t_i \in [t_0, t_s]\right)$$
(4)

$$P_{fs}(t_0, t_s) = \Pr\left(\bigcup_{i=1}^{m} g_i(\mathbf{X}, t_i) < 0, \exists t_i \in [t_0, t_s]\right)$$
 (5)

where \cup and \cap stand for union intersection, respectively.

Component reliability analysis is required for system reliability analysis. Methods of time-dependent component reliability analysis include three groups: Rice's formula based

¹ 723 W. Michigan Street, Indianapolis, SL 260G, IN 46202, U.S.A., Tel: 1-317-278-3113, e-mail: duxi@iu.edu

methods [7-9], meta-model based methods [10-13], and methods which convert time-dependent into time-independent reliability. Rice's formula based methods are most commonly used [14]. For example, the PHI2 method [8] allows for time-variant reliability problems to be solved using classical time-invariant reliability method, the first order reliability method (FORM). Hu and Du then proposed the joint up-crossing rate method in estimating the time-dependent reliability [9]. Rice's formula-based methods prove more efficient than others but may lead to large errors if up-crossings are strongly dependent.

Higher accuracy can be achieved by meta-model based methods. Hu and Du introduced a mixed efficient global optimization method employing the adaptive Kriging-Monte Carlo simulation (MCS) so that this high accuracy is achieved [12]. Wang and Wang developed a nested extreme response surface method by employing Kriging for reliability analysis with time-variant performance characteristics [13]. This group of methods may result in a high computational cost if the dimension of the problem is high.

Converting a time-dependent problem into a time-independent counterpart is possible by using the extreme value of the limit-state function. The methods include the envelope function method [15], extreme value response method [16], and the composite limit-state function method [17]. Still, obtaining accurate distribution of the extreme value in an efficient way is complicated. Hu and Du recently employed sequential efficient global optimization (EGO) to transform the time-dependent reliability problem into a time-independent problem with a second order method. The Hessian matrix is approximated by a quasi-Newton approach. It uses the gradients of the limit-state function at the points before the MPP search converges to the MPP. The method is efficient, but it may not accurately approximate the Hessian matrix since the points may not be on the surface of the envelope function [18].

Many studies have been conducted on time-dependent system reliability as well. For instance, Song and Der Kiureghian developed a joint first-passage probability method based on the conditional distribution analysis in estimating the reliability of systems subjected to stochastic excitation [19]. Radhika et al. investigated nonlinear vibrating systems under stochastic excitations by implementing the asymptotic extreme value theory and Monte Carlo simulation (MCS) [20]. Yu et al. employed the combination of the extreme value moment and improved maximum entropy method to access the time-variant system reliability with temporal parameters [21]. Gong and Frangopol proposed a new efficient method for time-dependent reliability which is formulated as a large-scale series system consisting of time-independent response functions [22]. Hu and Mahadevan proposed a novel and efficient methodology for time-dependent system reliability by considering the system as an equivalent Gaussian random field [23].

Time-independent system reliability can be approximated by the multidimensional integration of the joint probability density function (PDF) of random variables once the marginal distributions and correlation coefficients of component states are obtained by the second and first order approximations [24]. Wu and Du proposed a method of predicting the time-independent system reliability by approximating the marginal distributions with the second order saddlepoint method (SOSPA) [25].

It is desirable to take advantages of time-dependent component reliability methods and time-independent system reliability methods. To this end, we integrate the second order saddlepoint approximation [18], which is for time-dependent component reliability analysis and the second order saddlepoint approximation for time-independent system reliability analysis. The new method approximates the joint probability density function of the evelope functions of component responses by a multivariate normal density, whose mean vector and covariance matrix are obtained by the second and first order approximations, respectively. The proposed method approximates the envelope function of a component limit-state function at the Most Probable Points (MPPs) of the envelope function with a full quadratic function, and this allows for the use of most popular reliability methods, including the first and second order reliability methods (FORM and SORM). The employment of the MPP and second order approximation makes the proposed method both efficient and accurate.

This paper is organized as follows: Section 2 reviews the first order reliability method for time dependent reliability analysis. Section 3 discusses the proposed method for time-dependent system reliability analysis. Section 4 presents three examples, and Section 5 provides conclusions and discusses the possible future work.

2. METHODOLOGY REVIEW

The second order time-dependent system reliability method is based several existing methods, which are reviewed in this section.

2.1 Time-Dependent Component Reliability

The limit-state function of a component is given in Eq. (1), and its reliability is therefore a function of time (or timespan) as indicated in Eq. (2). The most commonly used reliability method is FORM, which is reviewed below.

2.1.1 First Order Reliability Method

FORM is originally used for time-independent reliability analysis, and it can also be used for time-dependent reliability analysis. It converts a general non-Gaussian process response into an equivalent Gaussian process response. \mathbf{X} is at first transformed into standard normal variables \mathbf{U} . Then the most probable point (MPP) \mathbf{u}^* at t is identified by the following model:

$$\begin{cases}
\min \sqrt{\mathbf{U}\mathbf{U}^{\mathrm{T}}} \\
\text{s.t. } g(\mathbf{X}, t) = g(\mathbf{T}(\mathbf{U}), t) = 0
\end{cases}$$
(6)

where $T(\cdot)$ is an operator of the transformation from **U** to **X**. The limit-state function is linearized at $\mathbf{u}^*(t)$ by

$$g(T(\mathbf{U}),t) = g(\mathbf{u}^*,t) + \sum_{i=1}^{N} \frac{\partial g}{\partial U_i} \bigg|_{\mathbf{u}^*} (U_i - u_i^*)$$

$$= \nabla g(\mathbf{u}^*,t)(\mathbf{U} - \mathbf{u}^*)$$
(7)

where $\nabla g(\mathbf{u}^*,t) = \left[\frac{\partial g}{\partial U_1}\Big|_{\mathbf{u}^*}, ..., \frac{\partial g}{\partial U_N}\Big|_{\mathbf{u}^*}\right]^{\mathrm{T}}$ is the gradient, and

 u_i^* is the *i*-th component of \mathbf{u}^* .

Then the probability of failure is computed by

$$p_f = \Pr(g(\mathbf{X}, t) < 0, \exists t \in [t_0, t_s])$$

$$= \Pr(\beta(t) + \alpha(t)\mathbf{U} < 0, \exists t \in [t_0, t_s])$$
(8)

where $\beta(t)$ is the time-dependent reliability index,

$$\beta(t) = \|\mathbf{u}^*\| \tag{9}$$

and $\alpha(t)$ is the time-dependent unit gradient vector

$$\boldsymbol{\alpha}(t) = \frac{\nabla g(t)}{\|\nabla g(t)\|} = [\alpha_1(t), \alpha_2(t), \dots, \alpha_N(t)]^{\mathrm{T}}$$
(10)

As Eq. (7) shows, the non-Gaussian process $g(\mathbf{X},t)$ has been transformed into an equivalent Gaussian process represented as a sum of standard normal random variables. After this, many methodologies are available for solving for the probability of failure, such as the upcrossing rate method [8, 9] and MCS [26].

2.1.2 Sequential optimization with EGO

The time-dependent probability of failure can be evaluated by the extreme value of the limit-state function.

$$p_f(t_o, t_s) = \Pr(g(\mathbf{X}, t) < 0, \exists t \in [t_o, t_s])$$

$$= \Pr\left(\min_{t \in [t_o, t_s]} g(\mathbf{X}, t) < 0\right)$$
(11)

The extreme limit-state function is also known as envelope function [15] or the composite limit-state function [17], $\min_{t \in [t_0, t_s]} g(\mathbf{X}, t)$ is obtained by

$$G(\mathbf{X}) = \min_{t \in [t_0, t_s]} g(\mathbf{X}, t) = g(\mathbf{X}, \tilde{t}(\mathbf{X}))$$
(12)

where $G(\mathbf{X})$ is the global minimum value of $g(\mathbf{X},t)$ with respect to t. $G(\mathbf{X})$ is time independent and only depends on \mathbf{X} . \tilde{t} is the time instant when the global minimal value occurs. \tilde{t} is the function of \mathbf{X} .

$$\tilde{t} = \left\{ \tilde{t} \mid \min_{t \in [t_o, t_s]} g(\mathbf{X}, t) \right\}$$
 (13)

The envelope function $G(\mathbf{X})$ is a spatial surface that is tangent to all the instantaneous limit-state functions at different time instants \tilde{t} . Since it is hard to analytically obtain the envelope function $G(\mathbf{X})$, FORM is used to approximated $G(\mathbf{X})$. The MPP of the envelope function is obtained by

$$\begin{cases}
\min \sqrt{\mathbf{U}\mathbf{U}^{\mathrm{T}}} \\
\text{s. t. } \min_{t \in [t_{o}, t_{s}]} g(\mathbf{T}(\mathbf{U}), t) = 0
\end{cases} \tag{14}$$
Eq. (11) is a double loop optimization problem. The inner

Eq. (11) is a double loop optimization problem. The inner loop is the global optimization with respect to time t, while the outer loop is the MPP search with respect to \mathbf{U} . The double loop is decoupled into a sequential single-loop process.

The first cycle is FORM analysis, the MPP $\mathbf{u}_{(1)}^*$ at the initial time t_0 by

$$\begin{cases}
\min \sqrt{\mathbf{U}\mathbf{U}^{\mathrm{T}}} \\
\text{s.t. } g(\mathbf{T}(\mathbf{U}), t_0) = 0
\end{cases}$$
(15)

Then the time is updated by global optimization at $\mathbf{u}_{(1)}^*$, and the new time is denoted by $\tilde{t}^{(1)}$, which is given by

$$\tilde{t}^{(1)} = \mathop{\rm argmin}_{t \in [t_0,t_s]} g\left(T\!\left(\mathbf{u}_{(1)}^*,t \right) \right) \tag{16}$$
 In the next cycle, the new MPP $\mathbf{u}_{(2)}^*$ is located at the time

In the next cycle, the new MPP $\mathbf{u}_{(2)}^*$ is located at the time instant $\tilde{t}^{(1)}$ using Eq. (15). And then the time is updated to $\tilde{t}^{(2)}$ by performing global optimization at $\mathbf{u}_{(2)}^*$.

$$\tilde{t}^{(2)} = \underset{t \in t_o, t_s]}{\operatorname{argmin}} g\left(T(\mathbf{u}_{(2)}^*, t)\right)$$
(17)

The above process is repeated until convergence.

The Efficient Global Optimization (EGO) is employed to solve the time t [27]. EGO has been widely used in various areas because it can efficiently search for the global optimum [12, 28]. The task is to solve for the time so that $g(t) = g(T(\mathbf{u}_{MPP}), t)$ is minimized. With a number of training points, the function is approximated by the following surrogate model:

 $\hat{y} = g(t) = g(T(\mathbf{u}_{\text{MPP}}), t) = F(t)^{\text{T}} \gamma + Z(t)$ (18) where $F(t)^{\text{T}} \gamma$ is a deterministic term, F(t) is a vector of regression functions, γ is a vector of regression coefficients, and Z(t) is a stationary Gaussian process with zero mean and a covariance given by

$$Cov(Z(t_1), Z(t_2)) = \sigma_Z^2 R(t_1, t_2)$$
(19)

where σ_Z^2 is process variance, and $R(\cdot, \cdot)$ is the correlation function.

The output of the surrogate model is a Gaussian random variable following

$$\hat{y} = g(t) \sim N(\mu(t), \sigma^2(t)) \tag{20}$$

where $\mu(t)$ and $\sigma(t)$ are the mean and standard deviation of \hat{y} , respectively.

After building the initial model, the expected improvement (EI) metric is used to identify the new training point with the highest probability to produce a better extreme value of the response. The improvement is defined by

$$I = \max(y^* - y, 0)$$
 (21)

where $y^* = \min_{i=1,2,...,k} g(t_i)$ is the current minimum response obtained from the sample training points.

Thus its expectation or EI is computed by

$$EI(t) = E[\max(y^* - y, 0)]$$

$$= (y^* - \mu(t))\Phi\left(\frac{y^* - \mu(t)}{\sigma(t)}\right) + \sigma(t)\phi\left(\frac{y^* - \mu(t)}{\sigma(t)}\right)$$
(22)

where $\Phi(\cdot)$ and $\phi(\cdot)$ are the cumulative distribution function (CDF) and PDF of a standard normal variable, respectively.

The new training point t_{new} is identified as the time that maximizes the expected improvement.

$$t_{new} = \operatorname{argminEI}(t)$$
 (23)

The convergence criterion of EGO could be set to $\varepsilon_{\rm EI} = |y^*| \times 2\%$. By combining sequential strategy with EGO, the MPP \mathbf{u}^* of extreme limit-state function $G(\mathbf{X})$ can be obtained efficiently by solving Eq. (14). The probability of failure with FORM is estimated by

$$p_f(t_o, t_s) = \Pr(g(\mathbf{X}, t) < 0, \exists t \in [t_o, t_s])$$

$$= \Pr(G(\mathbf{X}) < 0) = \Phi(-\beta)$$
(24)

where $\beta = \|\mathbf{u}^*\|$ is the first order reliability index.

The method is named FORM since FORM is involved in Eq. (14). In general, the envelope function can be highly nonlinear

and FORM may not be accurate enough. Thus, a second order method is preferred and it uses envelope theorem to obtain the second order information of the extreme limit-state function. Then SOSPA is used to estimate the probability of failure.

PROPOSED METHOD 3.

3.1 Overview

The envelope function of a component (or limit-state function) is generally nonlinear as shown in Fig. 1. It is the reason we use a second order approximation for the envelope function. Specifically, we approximate the envelope function at its MPP with a quadratic function. As a result, we also need the gradient and the Hessian matrix of the envelope function at the MPP.

It is shown that the MPP of the envelope function is the worst-case MPP of the limit-state function on $[t_0, t_s]$ [18]. In other words, the MPP is the closest point between the origin and all the instantaneous limit-state functions on $[t_0, t_s]$. This is illustrated in Fig. 1. The MPP of the envelope function can be efficiently found using a sequential single loop method [18]. This MPP is also the MPP of the worst-case limit-state function; as a result, the gradient of the envelope function is equal to the gradient of the worst-case limit-state function [18].

The Hessian matrix of the envelope function, however, may not be the Hessian matrix of the worst-case limit-state function as shown in Fig. 1. The Hessian matrix of the envelope function can be approximated by the gradients of the instantaneous limitstate functions [18], but the second derivative of the envelope function with respect to time is not considered. The method in [18] may not always work. In this work, we derive analytical second derivatives of the envelope function with respect to both random input variables and time, and the Hessian matrix of the envelope function can then be obtained accurately.

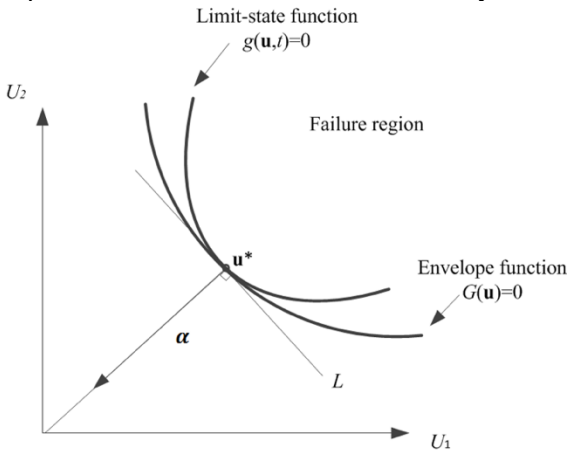


Fig. 1 Tangential relationship between limit-state function and envelope function

The general procedure of finding the second order information of the envelope is summarized below.

At first we employ the method in [18] to find the MPP of the envelope function using Eq. (14). Once we get the MPP of the envelope function, we know the gradient of the envelope because it is equal to the gradient of the limit-state function at the MPP. Next we determine the Hessian matrix of the envelope function with Eq. (35). The Hessian matrix consists of second derivatives of the limit-state function with respect to random input variables **X** and time t. The equations are derived in Sec. 3.2. Once the MPP, gradient and Hessian matrix are available, we use the second order saddlepoint approximation to find the probability of component failure and then perform system reliability analysis. The method hereby is denoted by SOSPA involved.

3.2 Hessian matrix of the envelope function

After the MPP of the envelope function is found, the quadratic envelope function is formulated as [25]

$$G(\mathbf{U}) = \mathbf{a} + \mathbf{b}^{\mathrm{T}}\mathbf{U} + \mathbf{U}^{\mathrm{T}}\mathbf{C}\mathbf{U}$$
 (25)

where

$$\begin{cases} a = \frac{1}{2} (\mathbf{u}^*)^{\mathrm{T}} \mathbf{H} \mathbf{u}^* - \nabla G(\mathbf{u}^*)^{\mathrm{T}} \mathbf{u}^* \\ \mathbf{b} = \nabla G(\mathbf{u}^*) - \mathbf{H} \mathbf{u}^* \\ \mathbf{C} = \frac{1}{2} \mathbf{H} = \operatorname{diag}(\tilde{c}_1, \tilde{c}_2, \dots, \tilde{c}_N) \end{cases}$$
(26)

 $\nabla G(\mathbf{u}^*) = \left(\frac{\partial G}{\partial U_1}\Big|_{\mathbf{u}^*}, \dots, \frac{\partial G}{\partial U_n}\Big|_{\mathbf{u}^*}\right) \quad \text{is the gradient of the}$ envelope function. $\ddot{\mathbf{H}}$ is the Hessian matrix, which is given by

$$\mathbf{H} = \begin{bmatrix} \frac{\partial^2 G}{\partial U_1^2} & \cdots & \frac{\partial^2 G}{\partial U_1 \partial U_n} \\ \vdots & \ddots & \vdots \\ \frac{\partial^2 G}{\partial U_n \partial U_1} & \cdots & \frac{\partial^2 G}{\partial U_n^2} \end{bmatrix}_{\mathbf{u}^*}$$
(27)

The envelope function $G(\mathbf{X}) = 0$ at \mathbf{u}^* is given by $G(\mathbf{U}) = \min_{t \in [t_0, t_s]} g(\mathbf{U}, t) = g(\mathbf{U}, \tilde{t})|_{\mathbf{u}^*}$ (28)

 \tilde{t} is the worst-case time instant, and it is found by

$$\dot{g}(\mathbf{U},t) = 0 \tag{29}$$

where \dot{g} is the derivative function of g with respect to t.

The first derivative of $G(\mathbf{U})$ with respect to a random input variable at \mathbf{u}^* is

$$\frac{\partial G}{\partial U_i} = \frac{\partial g}{\partial U_i} + \frac{\partial g}{\partial \tilde{t}} \frac{\partial \tilde{t}}{\partial U_i}$$
As $\dot{g}(\mathbf{U}, t) = 0$, Eq. (26) becomes

$$\frac{\partial G}{\partial U_i} = \frac{\partial g}{\partial U_i}$$
 (31) indicates the envelope function and the limit-state

function have the same gradient at u*. Then, the second derivative of $G(\mathbf{U})$ with respect random input random variables at \mathbf{u}^* is

$$\frac{\partial^2 G}{\partial U_i \partial U_j} = \frac{\partial}{\partial U_j} \left(\frac{\partial G}{\partial U_i} \right) = \frac{\partial}{\partial U_j} \left(\frac{\partial g}{\partial U_i} \right) \\
= \frac{\partial^2 g}{\partial U_i \partial U_j} + \frac{\partial^2 g}{\partial U_i \partial t} \frac{\partial t}{\partial U_j} \tag{32}$$

We then take the derivative of Eq. (26) with respect to U_i , it is given by

$$\frac{\partial \dot{g}}{\partial U_i} + \frac{\partial \dot{g}}{\partial t} \frac{\partial t}{\partial U_i} = 0 \tag{33}$$

$$\frac{\partial t}{\partial U_i} = -\frac{\partial \dot{g}}{\partial U_i} / \frac{\partial \dot{g}}{\partial t} \tag{34}$$

By taking Eq. (29) and (34) into Eq. (32), the Hessian matrix **H** at \mathbf{u}^* and \tilde{t} can be expressed as

$$\left. \frac{\partial^2 G}{\partial U_i \partial U_j} \right|_{\mathbf{u}^*, \tilde{t}} = \frac{\partial^2 g}{\partial U_i \partial U_j} \right|_{\mathbf{u}^*, \tilde{t}} - \frac{\partial^2 g}{\partial U_i \partial t} \frac{\partial^2 g}{\partial U_j \partial t} / \frac{\partial^2 g}{\partial t^2} \right|_{\mathbf{u}^*, \tilde{t}} \tag{35}$$

In this case, the finite difference method is used to obtain the gradient and Hessian matrix of the envelope function.

Next, the second order saddlepoint approximation is employed to estimate the probability of failure. Saddlepoint approximation has several excellent features. It yields an accurate probability estimation, especially in the tail area of a distribution [29, 30].

The cumulant generating function (CGF) is formulated as

$$K(s) = -\beta s + \frac{1}{2}s^2 - \frac{1}{2}\sum_{i=1}^{n-1}\log(1 - 2sk_i)$$
 (36)

where $k_i = \tilde{c}_i$

The derivatives of CGF are

$$K'(s) = -\beta + s + \sum_{i=1}^{n-1} \frac{k_i}{1 - 2sk_i}$$
 (37)

$$K''(s) = 1 + \sum_{i=1}^{n-1} \frac{k_i^2}{(1 - 2sk_i)^2}$$
 (38)

The saddlepoint s_s is obtained by solving the following equation:

$$K'(t) = -\beta + s + \sum_{i=1}^{n-1} \frac{k_i}{1 - 2sk_i} = 0$$
 (39)

Then the probability of failure is evaluated by

$$p_f(t_o, t_s) = \Pr(g(\mathbf{X}, t) < 0, \exists t \in [t_o, t_s])$$

$$= \Phi(w) + \phi(w) \left(\frac{1}{w} - \frac{1}{v}\right) \tag{40}$$

where

$$w = \operatorname{sgn}(t_s) \{ 2[-K(t_s)] \}^{\frac{1}{2}}$$
 (41)

$$v = t_s [K''(t_s)]^{\frac{1}{2}}$$
 (42)

in which $sgn(s_s) = +1$, -1 or 0, depending on whether s_s is positive, negative, or zero.

The detailed steps of SOSPA are summarized below.

Step 1: Set k = 1, the initial time instant express as the initial extreme value time $\tilde{t}^{(0)} = t_0$, the initial MPP $\mathbf{u}_{(1)}^* = \mathbf{u}_0$ is a unit vector.

Step 2: Search for the MPP at time instant $\tilde{t}^{(k-1)}$ and obtain MPP $\mathbf{u}_{(k)}^*$ by solving the formulas

$$\begin{cases}
\min \sqrt{\mathbf{U}\mathbf{U}^{\mathrm{T}}} \\
\text{s. t. } g(\mathbf{T}(\mathbf{U}), \tilde{t}^{(k-1)}) = 0
\end{cases}$$
(43)

Step 3: Determine the optimal time $\tilde{t}^{(k)}$ by implementing EGO method with $\mathbf{u}_{(k)}^*$.

Step 4: Determine the gradient $\nabla G^{(k)}$ and Hessian matrix $\mathbf{H}^{(k)}$ of the envelope function at $\mathbf{u}_{(k)}^*$.

Step 5: Calculate p_f using SOSPA based on the information $(\mathbf{u}_{(k)}^*, \nabla G^{(k)}, \mathbf{H}^{(k)})$.

However, the proposed method does not work when the extreme value of the limit-state function occurs at the beginning or end of the time period. The is because the limit-state function $g(\mathbf{X},t)$ is not differentiable at the beginning or end point of the time period. In other words, the Eq. (29) is invalid when the optimal time instant of the extreme value function occurs at the beginning and end point of the time period $[t_o, t_s]$. As a result, the Hessian matrix derivative Eq. (35) is not true for the above

3.3 System reliability with SOSPA

In this section, we discuss how to extend SOSPA for time dependent component reliability to time dependent system reliability analysis.

System reliability can be estimated by integrating the joint PDF of all responses in the safe region. To use SOSPA, we consider the PDF of component responses directly. The system state is determined by component states predicted from component limit-state functions $Y_i = g_i(\mathbf{X}, t)$ (i = 1, 2, ... m).

Given all the limit-state functions with time, the series system is then determined by the

$$R_{S} = \Pr\left(\bigcap_{i=1}^{m} Y_{i} = g_{i}(\mathbf{X}, t) > 0, i = 1, 2, ..., m\right)$$
 (44)

Eq. (44) enable us to consider component reliability and dependencies since it needs the joint PDF $f_Y(y)$ of Y = $(Y_1, Y_2, ..., Y_m)$. Hereby, it is an alternative way to predict the system reliability that the joint PDF $f_{V}(y)$ is approximated by a multivariate normal distribution.

If we only consider the first order term of the extreme limitstate function Eq. (25), it becomes as follows:

$$G_i(\mathbf{U}) = -\nabla G(\mathbf{u}_i^*)^{\mathrm{T}} \mathbf{u}_i^* + \nabla G(\mathbf{u}_i^*) \mathbf{U}$$
(45)

If we divide both sides of Eq. (45) by the magnitude of the gradient, we obtain

$$\frac{G_i(\mathbf{U})}{\|\nabla G(\mathbf{u}_i^*)\|} = -\frac{\nabla G_i(\mathbf{u}_i^*)^{\mathrm{T}}}{\|\nabla G(\mathbf{u}_i^*)\|} \mathbf{u}_i^* + \frac{\nabla G_i(\mathbf{u}_i^*)}{\|\nabla G(\mathbf{u}_i^*)\|} \mathbf{U}$$
(46)

or

$$\frac{G_i(\mathbf{U})}{\|\nabla G(\mathbf{u}_i^*)\|} = -\beta_i + \alpha_i \mathbf{U}$$
 (47)

The event of the safe component $G_i(\mathbf{U}) > 0$ is equivalent to the event $-\beta_i + \alpha_i \mathbf{U} > 0$. We then define a new variable

$$Z_i = -\beta_i + \alpha_i \mathbf{U} \tag{48}$$

where
$$\alpha_i$$
 is the directional vector and is given below
$$\alpha_i = \frac{\nabla G_i(\mathbf{u}_i^*)}{\|\nabla G(\mathbf{u}_i^*)\|}$$
(48)
$$\alpha_i = \frac{\nabla G_i(\mathbf{u}_i^*)}{\|\nabla G(\mathbf{u}_i^*)\|}$$

 Z_i is an equivalent component response. It is obvious that Z_i follows a normal distribution. As a result, all the equivalent component responses follow a multivariate normal distribution if the envelope functions of all the components are linearized at their MPPs. The system reliability is then approximated by

$$R_{\mathcal{S}} = \Pr\left(\bigcap_{i=1}^{m} Z_i(\mathbf{U}) > 0\right) = \Pr\left(\bigcap_{i=1}^{m} = -\beta_i + \alpha_i \mathbf{U} > 0\right) (50)$$

As a result, $\mathbf{Z} = (Z_1, Z_2, ..., Z_m)$ follows a multivariate normal distribution denoted by $N(\mu_Z, \Sigma_Z)$, where μ_Z is the mean vector and Σ_Z is the covariance matrix. System reliability

thus becomes the CDF
$$\Phi_m(\mathbf{0}; -\boldsymbol{\mu}_Z, \boldsymbol{\Sigma}_Z)$$
 of \mathbf{Z} at $\mathbf{0}$; namely
$$R_S = \Phi_m(\mathbf{0}; -\boldsymbol{\mu}_Z, \boldsymbol{\Sigma}_Z) = \int_{-\infty}^0 \cdots \int_{-\infty}^0 f_Z(\mathbf{z}) d\mathbf{z}$$
(51)

where $f_z(\mathbf{z})$ is the joint PDF of **Z** and the joint PDF of **Z** = $(Z_1, Z_2, ..., Z_m)$ is expressed below

$$f_Z(\mathbf{z}) = \frac{1}{\sqrt{(2\pi)^m |\mathbf{\Sigma}_Z|}} \exp\left(-\frac{(\mathbf{z} - \mathbf{u}_Z)^T \mathbf{\Sigma}^{-1} (\mathbf{z} - \mathbf{u}_Z)}{2}\right)$$
(52)

The accuracy of the mean vector μ_z and covariance matrix Σ_Z determine the accuracy of the multivariate normal integration in Eq. (52). In order to improve the accuracy of the Eq. (52) with high efficiency, the SOSPA method and the FORM are engaged in determining μ_Z and Σ_Z , respectively. Since the SOSPA is in general more accurate than the traditional FORM, the new method has higher accuracy. We use the SOSPA to approximate the marginal CDF of Z_i at 0, which is the component reliability

$$R_{\text{SPA}i} = \Pr(Z_i > 0) \tag{53}$$

where $R_{\rm SPAi}$ is SOSPA method given in Eq. (40). Then the associated reliability index is determined by

$$\beta_{\text{SPA}i} = \Phi^{-1}(R_{\text{SPA}i}) \tag{54}$$

 $\beta_{\rm SPA\it{i}} = \Phi^{-1}(R_{\rm SPA\it{i}})$ and $\beta_{\rm SPA\it{i}}$ is an equivalent reliability index.

Since β_{SPA} is estimated in a more accurate reliability way, we use it to replace β in Eq. (47). The mean vector of the multivariable distribution of Z becomes

$$\mathbf{u}_Z = (\beta_{\text{SPA1}}, \dots, \beta_{\text{SPA}m}) \tag{55}$$

The above treatment ensures that the component reliability or the marginal distributions of component responses are accurately estimated by the sequential efficient global optimization with the second order approximation. Simplified computation and high efficiency can be achieved by using the first order approximation with Eq. (49) to estimate the covariance matrix Σ_Z [25, 31]. Let the components of Σ_Z be $\rho_{ij} (i \neq j, i, j = 1, 2, ..., m)$, The covariance is given by

$$\rho_{ii} = \boldsymbol{\alpha}_i^{\mathrm{T}} \boldsymbol{\alpha}_i \tag{56}$$

$$(i \neq j, i, j = 1, 2, ..., m), \text{ The covariance is given by}$$

$$\rho_{ij} = \boldsymbol{\alpha}_i^{\mathsf{T}} \boldsymbol{\alpha}_j \tag{56}$$
Then $\boldsymbol{\Sigma}_Z$ is given by
$$\boldsymbol{\Sigma}_Z = \begin{bmatrix} 1 & \cdots & \rho_{1m} \\ \vdots & \ddots & \vdots \\ \rho_{m1} & \cdots & 1 \end{bmatrix}_{m \times m} \tag{57}$$
With \mathbf{u} and $\boldsymbol{\Sigma}_Z$ equilable, the question reliability \boldsymbol{P}_Z with

With \mathbf{u}_Z and $\mathbf{\Sigma}_Z$ available, the system reliability R_s with time can be easily calculated by integrating the PDF in Eq. (52) from $(-\infty, ..., -\infty)$ to (0, ..., 0) and the time dependent probability of system failure is

$$p_{fs} = 1 - R_s \tag{58}$$

Many methods such as the first order multi-normal approximation (FOMN) [32] and Alan Genz method [33] are developed to integrate $f_z(\mathbf{z})$ in Eq. (52).

The proposed method provides a new way to estimate the time dependent system reliability with nonlinear limit-state functions. The dependencies between component responses are automatically accommodated in the system covariance matrix, and component marginal CDFs can be obtained accurately using

the sequential efficient global optimization with second-order SPA method. This method not only achieves high accuracy in estimating system reliability but also simplifies the computations while maintaining high efficiency.

The procedure of the system reliability analysis with the SOSPA is briefly summarized below. The flowchart of this procedure is illustrated in Fig. 2.

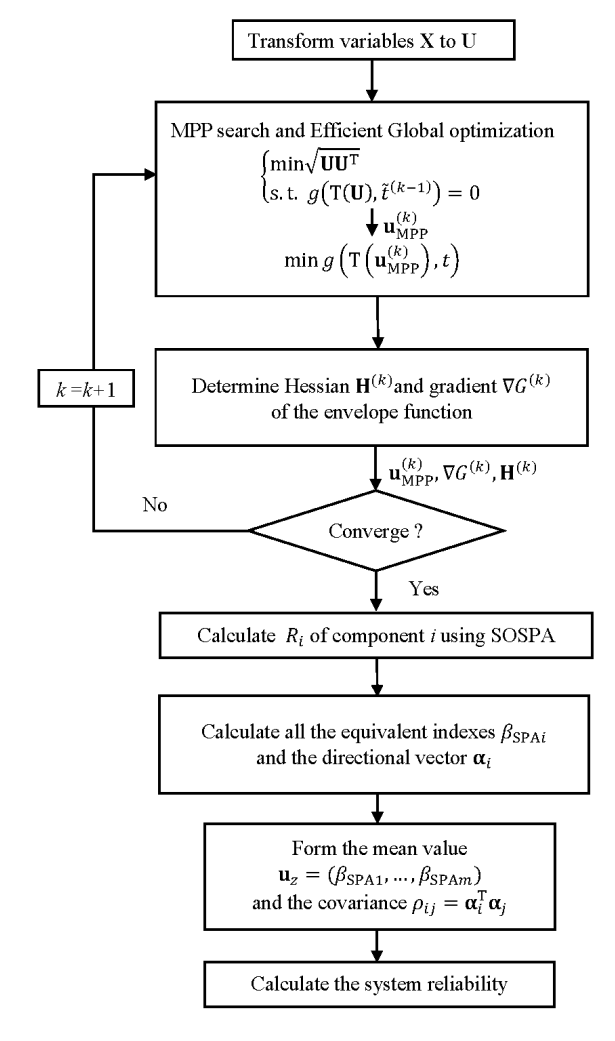


Fig.2 Flowchart of time-dependent system reliability

Step 1: Transform random variables X into U in the standard normal space.

Step 2: Search for MPPs $\mathbf{u}_{(k)}^*$, obtain the optimal time $\tilde{t}^{(k)}$ of the component limit-state function with the efficient global optimization method. The process is repeated until it is convergent at iteration k.

Step 3: Determine gradient $\nabla G^{(k)}$ and Hessian matrix $\mathbf{H}^{(k)}$ of the envelope function.

Step 4: Calculate component probability of failure based on the above component information $(\mathbf{u}_{(k)}^*, \nabla G^{(k)}, \mathbf{H}^{(k)})$, and use SOSPA result to find the mean of equivalent component responses.

Step 5: Repeat step 2-step 5 to analyze all components in system.

Step 6: Use respective MPPs and reliability indexes to find the system covariance matrix.

Step 7: Form the multivariate normal PDF and integrate it to obtain time dependent system reliability.

4. EXAMPLES

In this section, three examples are presented to test SOSPA for system reliability analysis. Example 1 is a mathematical problem which is used to demonstrate the details of the proposed method. Example 2 and 3 are engineering problems. The accuracy is measured by the percentage error with respect to a solution from MCS. The error is calculated by

$$\varepsilon = \frac{\left| p_{fs} - p_{fs}^{\text{MCS}} \right|}{p_{fs}^{\text{MCS}}} \times 100\%$$
 (59)

where p_{fs} is the result from SOSPA or FORM and p_{fs}^{MCS} is the result from MCS. We also use the number of function calls as a measure of efficiency.

4.1 Example 1: A math problem

A series system consists of two components with random basic variables $\mathbf{X} = (X_1, X_2)$. X_i (i = 1,2) is normally distributed with parameter $\mu_i = 3.5$ and $\sigma_i = 0.3$. The two limit-state functions are given by

$$g_{1}(\mathbf{X},t) = X_{1}^{2}X_{2} - 5X_{1}t + (X_{2} + 1)t^{2} - 8.2$$

$$g_{2}(\mathbf{X},t) = (\cos(5^{\circ})X_{1} + \sin(5^{\circ})X_{2})^{2}(-\sin(5^{\circ})X_{1} + \cos(5^{\circ})X_{2}) - 5(\cos(5^{\circ})X_{1} + \sin(5^{\circ})X_{2})t + ((-\sin(5^{\circ})X_{1} + \cos(5^{\circ})X_{2} + 1)t^{2} - 3.9$$
where t varies within $[0,5]$. (61)

Fig. 3 shows the parabolic curve of the envelope function of $g_1(\mathbf{X},t)$ formed by the instantaneous limit-state surface at different discretized time instants within the interval [0,5]. The contours of the analytical envelope functions of g_1 and g_2 are plotted in Fig. 4. The shaded area represents the system failure region.

In order to explain clearly how the SOSPA method works, we only show the details for $g_1(\mathbf{X},t)$. First, the MPP of the envelope function at \tilde{t} is obtained using sequential EGO. The iteration history is shown in Table 1. Once the iteration is convergent, the MPP is found at (-1.0714, -3.1172).

Table 1 Iteration history of MPP search for g_1

Iterations	u*	$ ilde{t}$
1	(-6.1450, -1.7052)	1.4735
2	(-2.1526, -2.9252)	1.9689
3	(-1.3877, -3.0305)	2.1483
4	(-1.1631, -3.0878)	2.2063
5	(-1.0941, -3.1096)	2.2251
6	(-1.0714, -3.1172)	2.2314

The probabilities of failure for g_1 and g_2 from SOSPA are $p_{f1} = 6.0040 \times 10^{-4}$ and $p_{f2} = 7.2248 \times 10^{-4}$. The mean values of the two equivalent component responses $\mathbf{Z} = (Z_1, Z_2)$ are then given by $\mathbf{u}_z = \mathbf{\beta}_{\text{SOSPA}} = (-3.2387, -3.1855)$.

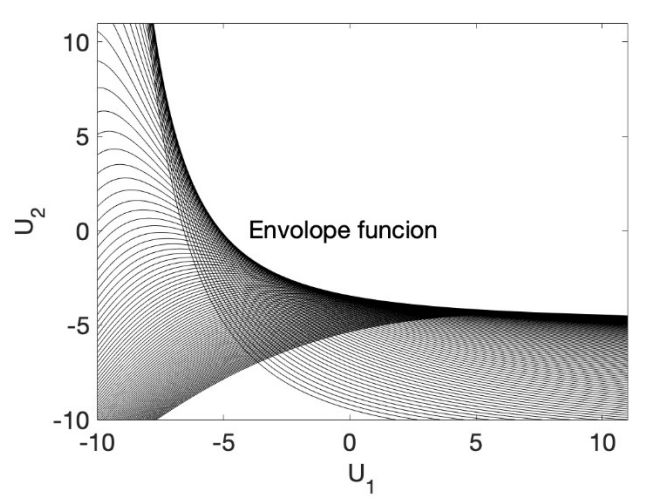


Fig.3 Envelope function formed by instantaneous limit-state surfaces

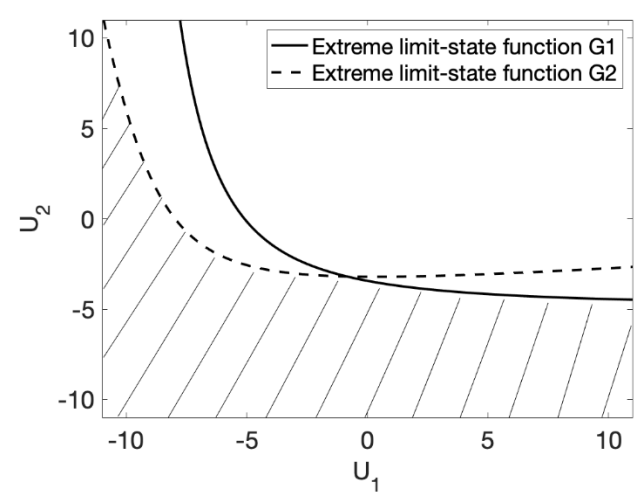


Fig.4 System extreme limit-state function

The unit directional vectors of the two limit-state functions are $\alpha_1 = (0.3254, 0.9456)$ and $\alpha_2 = (0.0098, 1.0)$. Thus, the correlation coefficient between g_1 and g_2 is $\rho_{12} = \alpha_1 \alpha_2^T = 0.9487$, and the covariance matrix is obtained as follow.

$$\mathbf{\Sigma}_{\mathbf{z}} = \begin{bmatrix} 1 & \rho_{12} \\ \rho_{21} & 1 \end{bmatrix} = \begin{bmatrix} 1 & 0.9487 \\ 0.9487 & 1 \end{bmatrix}$$
 The probability of system failure from SOSPA is $p_{fs} = 1 - 1$

The probability of system failure from SOSPA is $p_{fs} = 1 - R_s = 9.4747 \times 10^{-4}$. When FORM is used, the covariance is the same as Σ_z , and the mean values of the two equivalent component responses are below

$$\mathbf{u}_{z} = \mathbf{\beta}_{FORM} = (-3.2963, -3.2079).$$

The probability of system failure from FORM is $p_{fs} = 8.3738 \times 10^{-4}$. The MCS solution with a sample size of 10^6 is also obtained. For MCS, the time interval [0,5] is discretized evenly into 100 time instants. The total number of function calls

is therefore 10⁸. The results are shown in Table 2 where the errors calculated by Eq. (59) are given in brackets. Table 2 shows that SOSPA is much more accurate than FORM which produces a large error due to the nonlinearity of the envelope functions.

Table 2 Probability of system failure in Example 1

Methods	SOSPA	FORM	MCS
p_{f1}	6.0040×10^{-4} (1.57%)	4.8989×10^{-4} (19.69%)	6.10×10^{-4}
p_{f2}	7.2248×10^{-4} (1.03%)	6.6864×10^{-4} (8.41%)	7.30×10^{-4}
p_{sf}	9.4747×10^{-4} (3.32%)	8.3738×10^{-4} (14.6%)	9.80×10^{-4}

4.2 Example 2: A roof truss structure

A roof truss problem [25] is modified as our second example. The top boom and all the compression bars of the bar are made of concrete while the bottom boom and all the tension bars are made of steel. The bars bear a uniformly distributed load $q(t) = q_o(0.1\sin(0.25t) + 0.9)$, $t \in [0,10]$ years. A_C and E_C are the cross sectional area and elastic modulus of the concrete bars, respectively. A_S and E_S are the cross sectional area and elastic modulus of the steel bars, respectively. All parameters are independent and are listed in Table 3.

Table 3 Distribution of random variables

Variable (Unit)	Mean	Standard deviation	Distribution
$q_o(N/m)$	14000	1680	Normal
L(m)	12	0.12	Normal
$A_{\mathcal{S}}(\mathrm{m}^2)$	9.0×10^{-4}	9.0×10^{-5}	Normal
$A_{\mathcal{C}}(\mathrm{m}^2)$	5×10 ⁻²	5×10 ⁻³	Normal
$E_S(N/m^2)$	2×10^{11}	2×10^{10}	Normal
$E_C(N/m^2)$	3×10^{10}	3×10 ⁹	Normal
$f_S(N/m^2)$	3.35×10^{8}	6.7×10^7	Normal
$f_C(N/m^2)$	1.34×10^7	2.68×10^6	Normal

The perpendicular deflection of the roof peak node is calculated by

$$\Delta C = \frac{q l^2}{2} \left(\frac{3.81}{A_C E_C} + \frac{1.13}{A_S E_S} \right) \tag{62}$$

A failure occurs when the perpendicular deflection ΔC exceeds 1.37 cm. The limit-state function is then defined by

$$g_1(\mathbf{X}, t) = \frac{ql^2}{2} \left(\frac{3.81}{A_C E_C} + \frac{1.13}{A_S E_S} \right) - 0.0137 \tag{63}$$

The second failure mode is that the internal force of one bar exceeds its ultimate stress. The internal force of the bar is 1.185ql, and the ultimate strength of the bar is f_CA_C , where f_C is the compressive stress of the bar. The second limit-state function is then given by

$$g_2(\mathbf{X}, t) = 1.185ql - f_C A_C \tag{64}$$

The third failure occurs when the internal force of another bar 0.75ql exceeds its ultimate stress f_SA_S , where f_S is the tensile strength of the bar. Therefore, the third limit-state function is formulated by

$$g_3(\mathbf{X}, t) = 0.75ql - f_S A_S \tag{65}$$

SOSPA produces the means the equivalent component responses and the covariance matrix as follows:

$$\begin{split} & \pmb{\mu}_z = (-2.6083, -3.3940, -2.7237) \\ \pmb{\Sigma}_z = \begin{bmatrix} 1 & \cdots & \rho_{13} \\ \vdots & \ddots & \vdots \\ \rho_{31} & \cdots & 1 \end{bmatrix} = \begin{bmatrix} 1 & 0.1396 & 0.2846 \\ 0.1396 & 1 & 0.0463 \\ 0.2846 & 0.0463 & 1 \end{bmatrix} \end{split}$$

The probability of system failure from SOSPA is $pf_s = 8.0023 \times 10^{-3}$.

FORM and MCS are also used, and the results from the three methods are given in Table 4, showing that SOSPA has the higher accuracy than FORM with less efficiency.

Table 4 Probability of system failure in Example 2

Methods	SOSPA	FORM	MCS
p_{f1}	4.5497×10^{-3} (3.68%)	3.3738×10^{-3} (28.58%)	4.70×10^{-3}
p_{f2}	3.4434×10^{-4} (3.27%)	3.1805×10^{-4} (10.66%)	3.560×10^{-4}
p_{f3}	3.2279×10^{-3} (1.20%)	2.9547×10^{-3} (9.55%)	3.2670×10^{-3}
p_{sf}	8.0023×10^{-3} (2.26%)	6.5583×10^{-3} (19.9%)	8.1870×10^{-3}

4.3 Example 3: A Function Generator Mechanism System

Fig. 5 shows a function generator mechanism system, which can achieve a desire motion. This system consists of two function generator mechanisms [34].

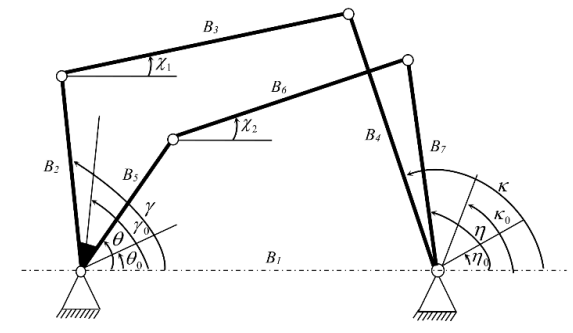


Fig. 5 A Function Generator Mechanism System

Mechanism 1 is a four-bar linkage mechanism with links B_1 , B_2 , B_3 , and B_4 , and it generates a sine function. Its motion error is the difference between the actual motion output and the required motion output. It is defined as

$$\varepsilon_1(\mathbf{X}_1, \gamma) = \kappa_a(\mathbf{X}_1, \gamma) - \kappa_d(\gamma) \tag{66}$$

where $\mathbf{X}_1 = (B_1, B_2, B_3, B_4)$ and links B_2 and B_5 are welded together. The two input angles satisfy

$$\gamma = 62^{\circ} + \theta \tag{67}$$

From the mechanism analysis, $\kappa_a(\mathbf{X}_1, \gamma)$ and $\kappa_d(\gamma)$ can be obtained by

$$\kappa_a(\mathbf{X}_1, \gamma) = 2 \arctan\left(\frac{-E_1 \pm \sqrt{E_1^2 + D_1^2 - F_1^2}}{F_1 - D_1}\right)$$
(68)

and

$$\kappa_d(\gamma) = 60^\circ + 60^\circ \sin\left(\frac{3}{4}(\gamma - 97^\circ)\right)$$
(69)

where $D_1=2B_4(B_1-B_2cos\gamma)$, $E_1=-2B_2B_4sin\gamma$, $F_1 = B_1^2 + B_2^2 + B_4^2 - B_3^2 - 2B_1B_2\cos\gamma.$

Mechanism 2 is the other four-bar linkage mechanism with links B_1 , B_5 , B_6 , and B_7 , and it generates a logarithm function. The motion error is given by

$$\varepsilon_2(\mathbf{X}_2, \theta) = \eta_a(\mathbf{X}_2, \theta) - \eta_d(\theta)$$
 (68)

where $\mathbf{X}_2 = (B_1, B_5, B_6, B_7)$.

follows:

$$\eta_a(\mathbf{X}_2, \theta) = 2 \arctan\left(\frac{-E_2 \pm \sqrt{E_2^2 + D_2^2 - F_2^2}}{F_2 - D_2}\right)$$
 (69)

$$\eta_d(\theta) = 60^{\circ} \log_{10} \frac{[(\theta + 15^{\circ})/60^{\circ}]}{\log_{10} 2}$$
 (70)

 $\eta_{d}(\theta) = 60^{\circ} \log_{10} \frac{[(\theta + 15^{\circ})/60^{\circ}]}{\log_{10} 2}$ (70) where $D_{2} = 2B_{7}(B_{1} - B_{5}cos\theta)$, $E_{2} = -2B_{5}B_{7}sin\theta$, and $F_{2} = B_{1}^{2} + B_{5}^{2} + B_{7}^{2} - B_{6}^{2} - 2B_{1}B_{5}cos\theta$.

Mechanism 1 is considered reliable if $\{e_2 < \varepsilon_1(\mathbf{X}_1, \gamma) < \epsilon_2 < \varepsilon_3(\mathbf{X}_2, \gamma) < \epsilon_3 < \epsilon_4 < \epsilon_5 < \epsilon_5$ e_1 }, where e_1 and e_2 are allowable motion errors with e_1 = 1.4 and $e_2 = -0.8$. When the motion error is positive, the limit-state function is defined by

$$g_1(\mathbf{X}_1, \gamma) = \varepsilon_1(\mathbf{X}_1, \gamma) - e_1 \tag{71}$$

As for the negative motion error, the limit-state function is given by

$$g_2(\mathbf{X}_1, \gamma) = \varepsilon_1(\mathbf{X}_1, \gamma) - e_2 \tag{72}$$

Similarly, the limit-state functions of mechanism 2 are as

$$g_3(\mathbf{X}_2, \theta) = \varepsilon_2(\mathbf{X}_2, \theta) - e_3 \tag{74}$$

$$g_4((\mathbf{X}_2, \theta)) = \varepsilon_2(\mathbf{X}_2, \theta) - e_4 \tag{75}$$

in which $e_3 = 1.0$ and $e_4 = -2.9$. The random variables are given in Table 5. The mechanism system performs its intended functions over an interval of $[\theta_0, \theta_s] = [45^{\circ}, 95^{\circ}]$. The system is a series system with four components (limit-state functions).

Table 5 Parameters in Example 2

Variable (Unit)	Mean	Standard deviation	Distribution
B_1 (mm)	100	0.3	Normal
$B_2(mm)$	55.5	0.05	Normal
B_3 (mm)	144.1	0.05	Normal
$B_4(\text{mm})$	72.5	0.05	Normal
$B_5(\text{mm})$	79.5	0.05	Normal
$B_6(\text{mm})$	203	0.05	Normal
$B_7(\text{mm})$	150.8	0.05	Normal

Table 6 shows the results. It indicates that the accuracy of SOSPA is in general better than FORM. However, both methods produce almost identical results for p_{f2} and p_{f4} . The reason is that the extreme values of two corresponding limit-state functions occur at the beginning of the time period (at 45°). Thus, the Hessian matrices of the two envelope functions are not accurate, and SOSPA is not accurate for p_{f2} and p_{f4} . Since the two probabilities of component failure are much smaller than the other two probabilities, their effect on the probability of system failure is insignificant.

Table 6 Probability of system failure in Example 3

	SOSPA	FORM	MCS
p_{f1}	6.8663×10^{-3} (1.09%)	5.6273×10^{-3} (18.94%)	6.9420×10^{-3}
p_{f2}	5.7646×10^{-5} (5.50%)	5.7646×10^{-5} (5.50%)	6.10×10^{-5}
p_{f3}	2.5156×10^{-3} (1.60%)	2.0×10^{-3} (19.20%)	2.4760×10^{-3}
p_{f4}	2.5460×10^{-6} (15.31%)	2.5460×10^{-6} (15.31%)	3.0×10^{-6}
p_{sf}	$7.1242 \times 10^{-3} $ (0.92%)	5.7465×10^{-3} (20.1%)	7.190×10^{-3}

CONCLUSION

The proposed time dependent system reliability method predicts system reliability with a second order approximation. It is therefore in general more accurate than the first order approximation methods. But it is less efficient than the latter methods due to the needs of second derivatives.

The new method converts a time dependent problem into a time independent problem by using the envelope function or the extreme value of a limit-state function over the time span under consideration. The most probable point (MPP) of the envelope is found with the help of efficient global optimization. Then the envelope function is approximated at the MPP with its gradient and Hessian matrix. The reliability of each component is calculated by the second order saddlepoint approximation, and the dependences between component responses are considered with the first approximation for the sake of efficiency. Once the estimated marginal component distributions and component correlations are available, the joint distribution of all the component responses is formed by a multivariate normal distribution, which leads to a fast evaluation of the system reliability.

The proposed envelope method works well if the envelope function is convex. The global MPP of the envelope function may not be found if the envelope function has multiple MPPs. For this case, the MPP search may start from different instants of time, and then the worst-case MPP is used. The proposed method does not work for a special case where the extreme value of a limit-state function occurs at the beginning or end of the period of time under consideration, and the reason is that the derivations of the Hessian matrix of the envelope function are for the case where the extreme value occurs inside the period of time.

Out future work will address the above two issues. The proposed method can also be further extended to time and space dependent problems where random processes and random fields are also involved.

ACKNOWLEDGEMENTS

We would like to acknowledge the support from the National Science Foundation under Grants No. 1923799 (formerly 1727329).

REFERENCES

- [1] Rausand, M., and Høyland, A., 2003, System reliability theory: models, statistical methods, and applications, John Wiley & Sons.
- [2] Hu, Z., and Du, X., 2014, "Lifetime cost optimization with time-dependent reliability," Engineering Optimization, 46(10), pp. 1389-1410.
- [3] Singh, A., Mourelatos, Z. P., and Li, J., 2010, "Design for lifecycle cost using time-dependent reliability," Journal of Mechanical Design, 132(9), p. 091008.
- [4] Wu, H., Zhu, Z., and Du, X., 2020, "System Reliability Analysis with Autocorrelated Kriging Predictions," Journal of Mechanical Design, 142(10), p. 101702.
- [5] Zhang, J., and Du, X., 2011, "Time-dependent reliability analysis for function generator mechanisms," Journal of Mechanical Design, 133(3), p. 031005.
- [6] Caprani, C. C., and OBrien, E. J., 2010, "The use of predictive likelihood to estimate the distribution of extreme bridge traffic load effect," Structural safety, 32(2), pp. 138-144.
- [7] Hu, Z., and Du, X., 2012, "Reliability analysis for hydrokinetic turbine blades," Renewable Energy, 48, pp. 251-262
- [8] Andrieu-Renaud, C., Sudret, B., and Lemaire, M., 2004, "The PHI2 method: a way to compute time-variant reliability," Reliability Engineering & System Safety, 84(1), pp. 75-86.
- [9] Hu, Z., and Du, X., 2013, "Time-dependent reliability analysis with joint upcrossing rates," Structural and Multidisciplinary Optimization, 48(5), pp. 893-907.
- [10] Hu, Z., Li, H., Du, X., and Chandrashekhara, K., 2013, "Simulation-based time-dependent reliability analysis for composite hydrokinetic turbine blades," Structural and Multidisciplinary Optimization, 47(5), pp. 765-781.
- [11] Hu, Z., and Mahadevan, S., 2016, "A single-loop kriging surrogate modeling for time-dependent reliability analysis," Journal of Mechanical Design, 138(6), p. 061406.
- [12] Hu, Z., and Du, X., 2015, "Mixed efficient global optimization for time-dependent reliability analysis," Journal of Mechanical Design, 137(5), p. 051401.
- [13] Wang, Z., and Wang, P., 2013, "A new approach for reliability analysis with time-variant performance characteristics," Reliability Engineering & System Safety, 115, pp. 70-81.
- [14] Rice, S. O., 1944, "Mathematical analysis of random noise," Bell System Technical Journal, 23(3), pp. 282-332.
- [15] Du, X., 2014, "Time-dependent mechanism reliability analysis with envelope functions and first-order approximation," Journal of Mechanical Design, 136(8), p. 081080.
- [16] Li, J., Chen, J., and Fan, W., 2007, "The equivalent extreme-value event and evaluation of the structural system reliability," Structural safety, 29(2), pp. 112-131.
- [17] Singh, A., and Mourelatos, Z. P., 2010, "On the time-dependent reliability of non-monotonic, non-repairable systems," SAE International Journal of Materials and Manufacturing, 3(1), pp. 425-444.
- [18] Hu, Z., and Du, X., "Second Order Reliability Method for Time-Dependent Reliability Analysis Using Sequential Efficient

- Global Optimization," Proc. ASME 2019 International Design Engineering Technical Conferences and Computers and Information in Engineering Conference, American Society of Mechanical Engineers Digital Collection.
- [19] Song, J., and Der Kiureghian, A., 2006, "Joint first-passage probability and reliability of systems under stochastic excitation," Journal of Engineering Mechanics, 132(1), pp. 65-77.
- [20] Radhika, B., Panda, S., and Manohar, C., 2008, "Time variant reliability analysis of nonlinear structural dynamical systems using combined Monte Carlo simulations and asymptotic extreme value theory," Computer Modeling in Engineering and Sciences, 27(1/2), p. 79.
- [21] Yu, S., Wang, Z., and Meng, D., 2018, "Time-variant reliability assessment for multiple failure modes and temporal parameters," Structural and Multidisciplinary Optimization, 58(4), pp. 1705-1717.
- [22] Gong, C., and Frangopol, D. M., 2019, "An efficient time-dependent reliability method," Structural Safety, 81, p. 101864.
- [23] Hu, Z., and Mahadevan, S., 2015, "Time-dependent system reliability analysis using random field discretization," Journal of Mechanical Design, 137(10), p. 101404.
- [24] Hohenbichler, M., and Rackwitz, R., 1982, "First-order concepts in system reliability," Structural safety, 1(3), pp. 177-188.
- [25] Wu, H., and Du, X., "System Reliability Analysis With Second Order Saddlepoint Approximation," Proc. ASME 2019 International Design Engineering Technical Conferences and Computers and Information in Engineering Conference, American Society of Mechanical Engineers Digital Collection.
- [26] Hu, Z., and Du, X., 2015, "Mixed efficient global optimization for time-dependent reliability analysis," Journal of Mechanical Design, 137(5), p. 051401.
- [27] Jones, D. R., Schonlau, M., and Welch, W. J., 1998, "Efficient global optimization of expensive black-box functions," Journal of Global optimization, 13(4), pp. 455-492.
- [28] Wang, Z., and Wang, P., 2012, "A nested extreme response surface approach for time-dependent reliability-based design optimization," Journal of Mechanical Design, 134(12), p. 121007.
- [29] Goutis, C., and Casella, G., 1999, "Explaining the Saddlepoint Approximation," American Statistician, 53(3), pp. 216-224
- [30] Hu, Z., and Du, X., 2018, "Saddlepoint approximation reliability method for quadratic functions in normal variables," Structural Safety, 71, pp. 24-32.
- [31] Zeng, P., Jimenez, R., Li, T., Chen, Y., and Feng, X., 2017, "Application of Quasi-Newton Approximation-Based SORM for System Reliability Analysis of a Layered Soil Slope," Geo-Risk 2017, pp. 111-119.
- [32] Gollwitzer, S., and Rackwitz, R., 1988, "An efficient numerical solution to the multinormal integral," Probabilistic Engineering Mechanics, 3(2), pp. 98-101.
- [33] Genz, A., 1992, "Numerical computation of multivariate normal probabilities," Journal of Computational and Graphical Statistics, 1(2), pp. 141-149.

[34] Hu, Z., Zhu, Z., and Du, X., 2017, "Time-Dependent System Reliability Analysis for Bivariate Responses," ASCE-ASME Journal Risk and Uncerty in Engineering Systems, Part B: Mechanical Engineering, 4(3), p.031002.